Contrib Mineral Petrol (2002) 143: 115–130
DOI 10.1007/s00410-001-0335-4

A. Brunsmann · G. Franz · W. Heinrich

Experimental investigation of zoisite–clinozoisite phase equilibria in the system $CaO–Fe_2O_3–Al_2O_3–SiO_2–H_2O$

Received: 18 May 2001 / Accepted: 2 November 2001 / Published online: 12 January 2002

Abstract The system $Ca_2Al_3Si_3O_{11}(O/OH)–Ca_2Al_2FeSi_3O_{11}(O/OH)$, with emphasis on the Al-rich portion, was investigated by synthesis experiments at 0.5 and 2.0 GPa, 500–800 °C, using the technique of producing overgrowths on natural seed crystals. Electron microprobe analyses of overgrowths up to >100 μm wide have located the phase transition from clinozoisite to zoisite as a function of P–T–X_{ps} and a miscibility gap in the clinozoisite solid solution. The experiments confirm a narrow, steep zoisite–clinozoisite two-phase loop in T–X_{ps} section. Maximum and minimum iron contents in coexisting zoisite and clinozoisite are given by $X_{ps}^{zo}(\max) = 1.9 * 10^{-4}T + 3.1 * 10^{-2}P - 5.36 * 10^{-2}$ and $X_{ps}^{czo}(\min) = (4.6 * 10^{-4} - 4 * 10^{-5}P)T + 3.82 * 10^{-2}P - 8.76 * 10^{-2}$ (P in GPa, T in °C). The iron-free end member reaction clinozoisite = zoisite has equilibrium temperatures of 185 ± 50 °C at 0.5 GPa and 0 ± 50 °C at 2.0 GPa, with $\Delta H_r^0 = 2.8 \pm 1.3$ kJ/mol and $\Delta S_r^0 = 4.5 \pm 1.4$ J/mol × K. At 0.5 GPa, two clinozoisite modifications exist, which have compositions of clinozoisite I ~0.15 to 0.25 X_{ps} and clinozoisite II >0.55 X_{ps}. The upper thermal stability of clinozoisite I at 0.5 GPa lies slightly above 600 °C, whereas Fe-rich clinozoisite II is stable at 650 °C. The schematic phase relations between epidote minerals, grossular-andradite solid solutions and other phases in the system $CaO–Al_2O_3–Fe_2O_3–SiO_2–H_2O$ are shown.

A. Brunsmann · G. Franz (✉)
Technische Universität Berlin,
Institut für Angewandte Geowissenschaften,
Str. des 17. Juni 135, Berlin, Germany
E-mail: gerhard.franz@tu-berlin.de
Tel.: +49-30-34122291
Fax: +49-030-34126617

A. Brunsmann · W. Heinrich
GeoForschungsZentrum Potsdam,
Projektbereich 4.1, Potsdam, Germany

Editorial responsibility: J. Hoefs

Introduction

Epidote minerals are major phases in metabasites, metagreywackes and calc-silicate rocks among others, and may even form monomineralic 'epidosites'. The most common members of this mineral group belong to the $Ca_2Al_2AlSi_3O_{11}(O/OH)–Ca_2Al_2Fe^{3+}Si_3O_{11}(O/OH)$ solid solution series of orthorhombic zoisite and monoclinic clinozoisite/epidote. The composition of the orthorhombic and monoclinic solid solutions can be expressed as the mole fraction X_{ps} of the $Ca_2Al_2Fe^{3+}Si_3O_{11}(O/OH)$ component with $X_{ps} = Fe^{3+}/(Fe^{3+} + Al\text{-}2)$ (Deer et al. 1986). In zoisite, X_{ps} is restricted to values <0.02, whereas monoclinic solid solutions show $X_{ps} = 0$ to 1 (Deer et al. 1986). In general, the iron-poor, optically positive members of the monoclinic solid solution series are called clinozoisite, whereas the iron-rich, optically negative ones are called epidote. For clearness and because this study focus on the iron-poor part of the system, we will use the term 'clinozoisite' for all monoclinic forms, regardless of their composition. Brunsmann (2000) found two zoisite modifications, zoisite I and zoisite II, with an isosymmetric displacive phase transition. Because his data suggest that zoisite with $X_{ps} > \sim 0.05$ is zoisite II and the differences between zoisite I and II are only minor, this phase transition is insignificant for this study and, therefore, we always refer to his zoisite II.

Zoisite and clinozoisite are stable from low to high temperature and extremely high pressure up to 6.5 GPa (Poli and Schmidt 1998). The iron-poor members can be regarded as the hydrated low-temperature and high-pressure equivalent of the anorthite component in a rock, similar to lawsonite, although with a much lower water content. Furthermore, clinozoisite is one of the most common Fe^{3+}-bearing silicates in Ca- and Al-rich rocks. From the geochemical point of view, zoisite and clinozoisite are interesting as carriers of the petrogenetically important trace elements Pb, Sr and the REE.

Phase equilibria in the system $CaO–Fe_2O_3–Al_2O_3–SiO_2–H_2O$ concerning the phase transition from clinozoisite to zoisite, the location of the clinozoisite–zoisite two-phase field in P–T–X_{ps} space and the possible existence of miscibility gaps in the orthorhombic and monoclinic solid solution series, have been discussed for a long time (Deer et al. 1986; Franz and Selverstone 1992). Experimental investigations into these matters by a number of authors (Holdaway 1972; Jenkins et al. 1983, 1985; Holland 1984; Prunier and Hewitt 1985; Fehr and Heuss-Aßbichler 1997; Heuss-Aßbichler and Fehr 1997) did not yield unequivocal results.

In this contribution we address the questions of how much iron can be incorporated into zoisite as a function of P and T, what is the iron content in clinozoisite coexisting with zoisite, and how does the clinozoisite–zoisite two-phase field in P–T–X_{ps} space look like. Moreover, we discuss the existence of a miscibility gap along the iron-poor portion of the monoclinic solid solution series as well as the phase relations between zoisite, clinozoisite, and other phases of the system in dependence of temperature.

Experimental and analytical techniques

Minerals were synthesized from oxide-hydroxide mixtures of SiO_2 (Chempur no. 006965, 99.99%), Al_2O_3 (Aldrich no. 1344-28-1, 99.99%), Fe_2O_3 (Merck, pa), and $Ca(OH)_2$ (Merck no. 2111, pa) in the presence of a 1 M $CaBr_2$ solution. Adding a halogen compound to the system enhances growth of the crystals, but does not influence the zoisite–clinozoisite phase equilibria, as long as the halogen does not enter into the crystal structures. Neither zoisite nor clinozoisite are known to contain significant amounts of F or Cl (Deer et al. 1986), and it can safely be assumed that the much larger Br also does not enter into the structures. The use of chloridic and bromidic solutions was successfully employed for the synthesis of amphiboles by Zimmermann et al. (1996) and Melzer et al. (1998). Oxides and hydroxides were weighted in stoichiometric amounts of the desired zoisite/clinozoisite composition plus 10 wt% SiO_2 in excess to assure quartz saturation. We added four seeds of natural zoisite ($X_{ps} = 0.0$) and clinozoisite ($X_{ps} = 0.50 \pm 0.05$), each, to all runs, following Prunier and Hewitt (1985). The seed crystals were in the order of a few 100 μm in size and acted as substrates for overgrowths, which were large enough for detailed electron microprobe (EMP) analyses. The seed crystals contain some Mn and V in clinozoisite and V in zoisite (variety tanzanite), which are not present in the synthetic system and were used to distinguish between overgrowths and seed crystals in EMP analyses.

Bulk compositions on the join $Ca_2Al_3Si_3O_{11}(O/OH)–Ca_2Al_2FeSi_3O_{11}(O/OH)$, expressed as X_{ps} of the corresponding zoisite/clinozoisite composition, vary between $X_{ps}^{bulk} = 0.0$ and 1.0 in the 0.5-GPa runs, and between $X_{ps}^{bulk} = 0.2$ and 0.4 in the 2.0-GPa runs (Table 1). Oxygen fugacity was buffered by conventional double capsule technique with a solid state hematite–magnetite buffer, mixed in a ratio of 9:1. For hydrothermal runs, inner Pt capsules contained about 40 mg solids and 25 μl fluid, and outer Au capsules about 200 mg hematite–magnetite mixture and 200 μl H_2O. For piston cylinder runs AB P1 to AB P6, we used inner $Ag_{70}Pd_{30}$ capsules with approximately 20 mg solids and 5 μl fluid, and outer Au capsules with about 200 mg hematite–magnetite mixture and 20 μl H_2O. For piston cylinder runs AB P7 to AB P10 inner capsules consist of Au with about 30 mg solids and 10 μl fluid, and the outer capsules of Ag with about 400 mg hematite–magnetite mixture and 40 μl H_2O (for more details, see Brunsmann 2000).

Hydrothermal runs (Table 1) were performed in conventional cold seal hydrothermal vessels with horizontally positioned autoclaves and water as a pressure medium. The error in pressure is estimated to be ±10 MPa. Temperature was measured with Ni–Cr–Ni-thermocouples in approximately 4 mm distance from the capsule, and the total error of temperature is less than ±10 °C. First, the vessel was pressurized to 0.5 GPa followed by isobaric heating up to run temperature. At the end of the runs, samples were quenched isobarically with air to room temperature in less than 3 min. For piston cylinder runs (Table 1), we used a NaCl assembly with an internal graphite furnace. The error for pressure is ±50 MPa and the temperature is ±20 °C. First, a pressure of 1.7 GPa was applied, then the sample was heated to the required temperature with a heating rate of 100 °C/min, and finally the pressure was raised to 2.0 GPa. After 3–5 days, the runs were quenched to < 200 °C within less than 30 s.

After the runs, samples were checked for leakage, then opened and dried. The buffer material was checked optically and by X-ray methods for the presence of hematite and magnetite. Runs in which the buffer capacity was exhausted were rejected. The seed crystals were hand-picked and polished thin sections were prepared for electron microprobe analyses. The compositions of the overgrowths were measured along profiles from the seed crystals up to the border of the overgrowths. The optical distinction between zoisite and clinozoisite overgrowths was made by interference colour and extinction angle. The remaining sample material (from here on referred to as matrix) was analysed by powder X-ray diffraction.

Electron microprobe analyses were carried out with automated Cameca SX 100 and SX 50 electron microprobes at GFZ Potsdam. Measuring conditions were 15 kV, 15 nA, 20 s on peak of Kα and 10 s on background, using wollastonite (Si and Ca), synthetic corundum (Al), synthetic hematite (Fe), rhodonite (Mn) and vanadinite (V) as standard materials. The correction program used was the PAP software. Zoisite and clinozoisite mineral formulas were calculated on the basis of 12.5 oxygen assuming all Fe as Fe^{3+}. Only those analyses that yielded formulas in the range $Ca_{1.96–2.04}(Al,Fe^{3+})_{2.94–3.06}Si_{2.94–3.06}O_{11}(O/OH)$ have been accepted. Powder X-ray diffractograms were obtained with a Philips PW 1820 diffractometer at 20 to 60° 2Θ, step-scan mode with 0.02° 2Θ, 2 s per step. Diffractograms were evaluated with the X'Pert 1.2 software of Philips.

Results

Description of run products

The description of run products are shown in Table 1. At 0.5 GPa, the matrix assemblages generally consist of anorthite, garnet, quartz, zoisite and clinozoisite in variable amounts. Neither zoisite nor clinozoisite were found in the matrix in runs at 600 °C/$X_{ps}^{bulk} = 0.0$ and $= 0.05$ and 650 °C/$X_{ps}^{bulk} = 0.0$. In the run at 500 °C/$X_{ps}^{bulk} = 0.1$ scolecite was identified in trace amounts, and all runs with $X_{ps}^{bulk} = 1.0$ showed hematite as a matrix phase, but lacked anorthite. Runs with $X_{ps}^{bulk} = 0.0$, 0.125 and 0.2 at 500 °C, $X_{ps}^{bulk} = 0.0$ and 0.05 at 600 °C and $X_{ps}^{bulk} = 0.0$, 0.05 and 0.15 at 650 °C yielded no overgrowths. Coexisting zoisite and clinozoisite overgrowths on the respective seed crystals were found in four runs at 500 °C/$X_{ps}^{bulk} = 0.1$, 550 °C/$X_{ps}^{bulk} = 0.125$, 575 °C/$X_{ps}^{bulk} = 0.125$ and 600 °C/$X_{ps}^{bulk} = 0.1$; at 650 °C/$X_{ps}^{bulk} = 0.45$ only zoisite overgrowths were observed. All other runs at T = 500–650 °C/$X_{ps}^{bulk} = 0.15$ to 1.0 yielded exclusively clinozoisite

overgrowths. In general, both zoisite and clinozoisite overgrowths are ≥100 μm wide, their contacts to the seed crystals are always very sharp and the seed crystals lack resorption features (Fig. 1a–c, e). Only in the runs with $X_{ps}^{bulk} = 1.0$ and in the run with $X_{ps}^{bulk} = 0.6$ at 600 °C did the zoisite seed crystals clearly react with the rest of the charges and they were partly transformed into clinozoisite pseudomorphs (e.g. Fig. 1f).

In the runs at 2.0 GPa, the matrix assemblages are generally zoisite–clinozoisite–quartz, with garnet as an additional phase in most runs (Table 1). Quartz was not present in the run at 800 °C/$X_{ps}^{bulk} = 0.4$. No overgrowths were found in the runs at 600 °C. Coexisting zoisite and clinozoisite overgrowths on the respective seed crystals were formed in the runs with $X_{ps}^{bulk} = 0.2$ at 650, 700, 750 and 800 °C and in the run with $X_{ps}^{bulk} = 0.25$ at 750 °C. At 650 °C/$X_{ps}^{bulk} = 0.25$, 700 °C/$X_{ps}^{bulk} = 0.4$ and 800 °C/$X_{ps}^{bulk} = 0.4$, only clinozoisite overgrowths were found. The zoisite and clinozoisite overgrowths formed at 2.0 GPa do not differ in appearance from those formed at 0.5 GPa and their contacts to the seed crystals are also very sharp (Fig. 1d). In neither run were the seed crystals resorbed nor were the zoisite seed crystals partly transformed into clinozoisite pseudomorphs.

Composition of individual overgrowths

Representative compositional profiles of the overgrowths are shown in Fig. 2. All profiles show sharp compositional changes at the contact between seed

Table 1. Experimental conditions and run products for synthesis experiments of epidote minerals

Run No.	T (°C)	Composition[a] (X_{ps}^{bulk})	Duration (days)	Run products		
				Overgrowths[b]	Matrix[c]	Pseudomorphs
0.5-GPa runs						
AB 59	500	0.0	42	–	an, qtz, zo, (grt)	–
AB 55	500	0.1	42	zo + czo I	czo, qtz, (an), (sco)	–
AB 85	500	0.125	42	–	czo, grt, qtz, (zo)	–
AB 57	500	0.2	42	–	czo, grt, qtz	–
AB 58	500	0.25	42	czo I	czo, qtz, (grt)	–
AB 84	500	0.4	42	czo II	czo, grt, qtz	–
AB 88	500	0.6	42	czo II	grt, czo, qtz	–
AB 87	500	1.0	42	czo II	czo, grt, qtz, hm	yes
AB 74	550	0.125	42	zo + czo I	an, czo, qtz	–
AB 75	550	0.4	42	czo I + czo II	czo, grt, qtz	–
AB 76	550	0.6	42	czo II	czo, grt, qtz	–
AB 77	550	1.0	42	czo II	czo, grt, qtz, hm	yes
AB 95	575	0.125	28	zo + czo I	an, czo, qtz, (zo)	–
AB 96	575	0.35	28	czo II	czo, grt, qtz	–
AB 47	600	0.0	28	–	an, grt	–
AB 48	600	0.05	28	–	an, grt, qtz	–
AB 49	600	0.1	28	zo + czo I	an, czo, grt, qtz	–
AB 50	600	0.15	28	czo I	an, czo, grt, qtz	–
AB 51	600	0.2	28	czo I	an, czo, grt, qtz	–
AB 52	600	0.25	28	czo I + czo II	an, czo, grt, qtz	–
AB 91	600	0.6	21	czo II	czo, qtz, (grt)	yes
AB 92	600	1.0	21	czo II	czo, grt, qtz, (hm)	yes
AB 73	650	0.0	21	–	an, grt, qtz	–
AB 68	650	0.05	21	–	an, czo, grt, qtz	–
AB 70	650	0.15	21	–	an, czo, grt, qtz	–
AB 78	650	0.45	42	zo	an, czo, grt, qtz	–
AB 79	650	1.0	42	czo II	czo, grt, qtz, hm	yes
2.0-GPa runs						
AB P3	600	0.2	3	–	czo, zo, qtz	–
AB P4	600	0.4	3	–	czo, zo, qtz	–
AB P9	650	0.2	5	zo + czo	czo, zo, qtz, grt	–
AB P10	650	0.25	5	czo	czo, zo, qtz, grt	–
AB P1	700	0.2	3	zo + czo	czo, zo, qtz	–
AB P2	700	0.4	3	czo	czo, zo, qtz, grt	–
AB P7	750	0.2	3	zo + czo	czo, zo, qtz, (grt)	–
AB P8	750	0.25	3	zo + czo	czo, zo, qtz, (grt)	–
AB P5	800	0.2	4	zo + czo	czo, zo, qtz	–
AB P6	800	0.4	4	czo	czo, grt	–

[a] Composition on the join $Ca_2Al_3Si_3O_{11}(O/OH)$–$Ca_2Al_2Fe^{3+}Si_3O_{11}(O/OH)$ with 10 wt% excess SiO_2, $X_{ps} = Fe^{3+}/(Fe^{3+} + Al–2)$

[b] *zo* zoisite overgrowth; *czo* clinozoisite overgrowth (I and II refer to clinozoisite I and II at 0.5 GPa, see text)

[c] As determined by XRD and listed in order of abundance. *an* Anorthite; *czo* clinozoisite; *grt* garnet; *hm* hematite; *qtz* quartz; *sco* scolecite; *zo* zoisite; *( )* trace amounts

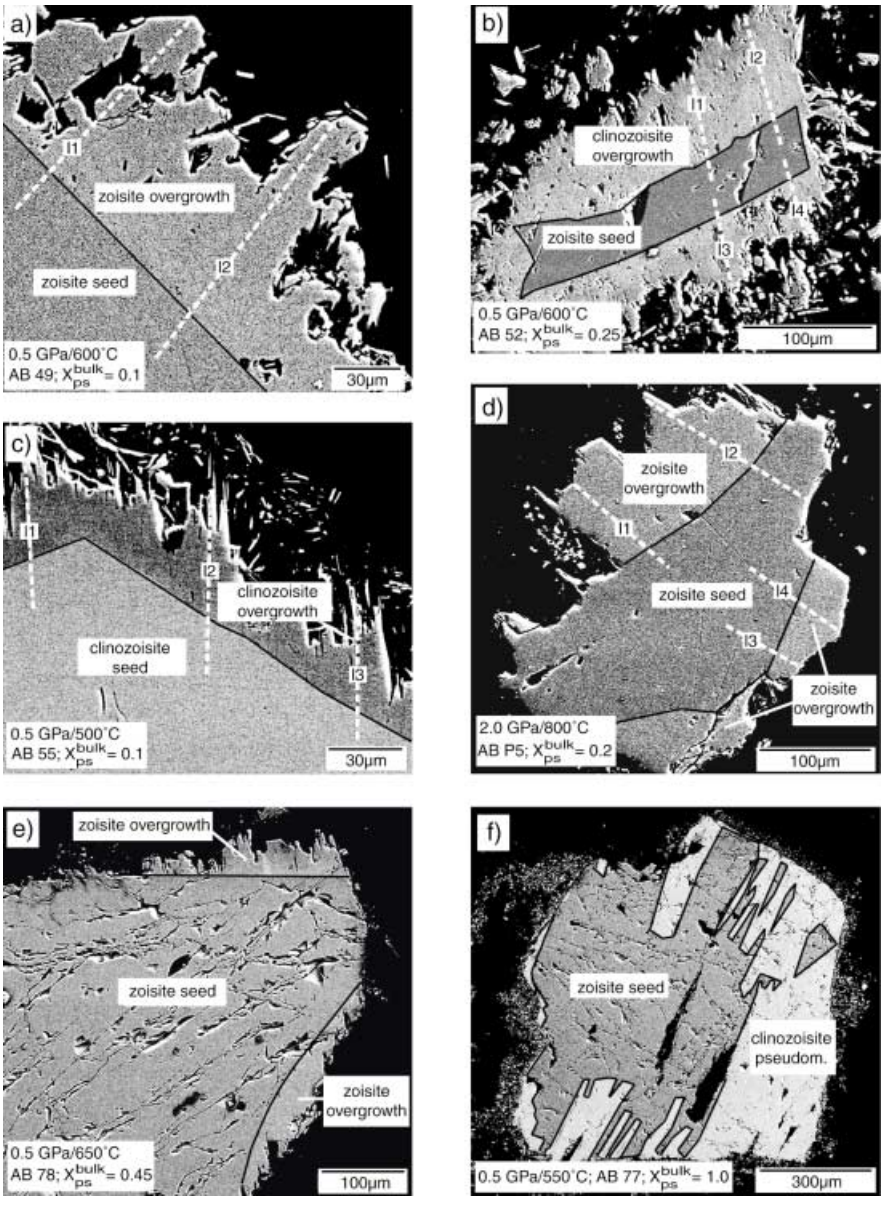

Fig. 1a–f. Back-scattered electron images from runs at 0.5 GPa (**a**–**c**, **e**, **f**) and 2 GPa (**d**), showing examples of overgrowths on **a**–**e** zoisite and clinozoisite seeds and **f** of a pseudomorph after a zoisite seed. *White dotted lines* in **a**–**d** indicate the positions of measured profiles shown in Fig. 2

crystal and overgrowth (Fig. 2). This is especially true for V and Mn, which are present in the seed crystals but are absent in the overgrowths. With respect to their Fe^{3+} contents and consequently X_{ps}, all overgrowths generally show an inner and outer zone (Fig. 2). The outer zones are relatively homogeneous, although they show some compositional scatter. Normally, this scatter is $< \pm 0.02$ X_{ps}, but might be as high as ± 0.07 X_{ps}, especially in the iron-rich runs (Table 2). The inner zones vary in widths between < 5 µm (Fig. 2b) and ~ 30 µm (Fig. 2a). They display large compositional scatter and have X_{ps} that differ from those of the corresponding outer zones, but that gradually approach the mean values of the outer zones with increasing distance from the seed crystals (e.g. Fig. 2a). In the case of zoisite overgrowths on zoisite seeds, the inner zones have higher iron contents than the outer zones (Fig. 2a, d), whereas in all other cases (clinozoisite overgrowths on zoisite seeds, Fig. 2b, and clinozoisite overgrowths on clinozoisite seeds, Fig. 2c) the iron contents of the inner zones are between those of the seed crystals and the outer zones.

Average composition of zoisite and clinozoisite overgrowths as a function of P, T and X_{ps}^{bulk}

For each run, we calculated the average zoisite and clinozoisite composition based on the outer parts of all zoisite and clinozoisite overgrowths of the respective runs. For the runs AB 75 and AB 52, in which the iron contents of the clinozoisite overgrowths cluster at two different X_{ps} values, we calculated the averages for each cluster. The resulting zoisite and clinozoisite compositions are listed in Table 2 and are shown in Fig. 3 for the 0.5-GPa runs and in Fig. 4 for the 2.0-GPa runs together with the corresponding X_{ps}^{bulk}.

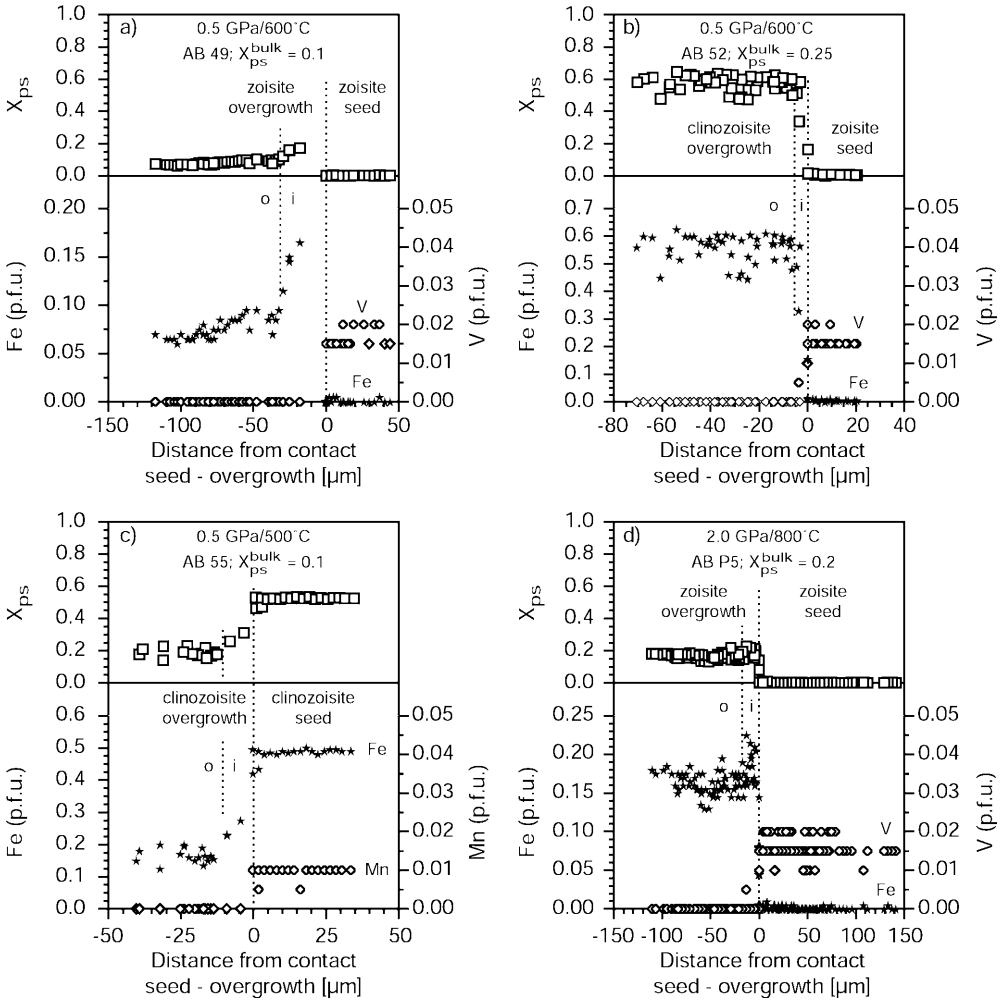

Fig. 2a–d. EMP analyses and representative compositional profiles from seeds to overgrowths. Data are compiled from profiles shown in Fig. 1a–d. The upper portions show X_{ps}, the lower portions the concentration of Fe^{3+}, V and Mn expressed as cations per formula unit, calculated on the basis of 12.5 O. Note the sharp steps in V and Mn, indicating that a chemical exchange between seed and overgrowth is restricted to < 10 μm. All overgrowths show a heterogeneous, up to 30-μm-wide inner zone (*i*) and a homogeneous outer zone (*o*)

Comparing the symmetries and X_{ps} of the overgrowths with the corresponding X_{ps}^{bulk} (Table 2; Figs. 3 and 4), we can distinguish four cases: (a) runs with coexisting zoisite and clinozoisite overgrowths and $X_{ps}^{zo} < X_{ps}^{bulk} < X_{ps}^{czo}$, (b) runs with two coexisting, compositionally different clinozoisite overgrowths czo I and czo II and $X_{ps}^{czoI} < X_{ps}^{bulk} < X_{ps}^{czoII}$, (c) runs with only clinozoisite overgrowths and $X_{ps}^{czo} \sim X_{ps}^{bulk}$, and (d) runs with one kind of overgrowth and small to remarkable differences between $X_{ps}^{overgrowth}$ and X_{ps}^{bulk}.

Case a

At both pressures, the iron content of coexisting zoisite and clinozoisite increases with increasing temperature (Table 2, Figs. 3 and 4). At 0.5 GPa, the iron content in zoisite increases from $X_{ps}^{zo} \sim 0.06$ at 500 °C to $X_{ps}^{zo} \sim 0.08$ at 600 °C, coexisting clinozoisite I has $X_{ps}^{czoI} \sim 0.16$ and ~ 0.20 (Fig. 3). At 2.0 GPa, the iron content in zoisite increases from $X_{ps}^{zo} \sim 0.13$ at 650 °C to $X_{ps}^{zo} \sim 0.16$ at 800 °C, coexisting clinozoisite has $X_{ps}^{czo} \sim 0.24$ and ~ 0.30 (Fig. 4). The two runs at 2.0 GPa/750 °C with $X_{ps}^{bulk} = 0.2$ and 0.25 show, within error, identical X_{ps}^{zo} and slightly different clinozoisite overgrowths with $X_{ps}^{czo} \sim 0.25$ and ~ 0.28.

Case b

The 0.5-GPa runs with $X_{ps}^{bulk} = 0.4$ at 550 °C and $X_{ps}^{bulk} = 0.25$ at 600 °C show coexisting clinozoisite I and clinozoisite II overgrowths with $X_{ps}^{czoI} \sim 0.20$ and $X_{ps}^{czoII} \sim 0.57$ at 550 °C and $X_{ps}^{czoI} \sim 0.21$ and $X_{ps}^{czoII} \sim 0.56$ at 600 °C.

Case c

At 0.5 GPa, the runs with $X_{ps}^{bulk} = 0.25$ and 0.6 at 500 °C, $X_{ps}^{bulk} = 0.6$ and 1.0 at 550 °C, and $X_{ps}^{bulk} = 0.2$ at 600 °C, yielded overgrowths with $X_{ps}^{overgrowth} \sim X_{ps}^{bulk}$ (Table 2, Fig. 3). The same is true for runs at 2.0 GPa with $X_{ps}^{bulk} = 0.4$ at 700 and 800 °C (Table 2, Fig. 4).

Case d

The runs with $X_{ps}^{bulk} = 0.4$ at 0.5 GPa/500 °C and $X_{ps}^{bulk} = 0.35$ at 0.5 GPa/575 °C yielded only clinozoisite II overgrowths with $X_{ps}^{overgrowth} > X_{ps}^{bulk}$ and $X_{ps}^{czoII} \sim 0.55$ and ~ 0.57, whereas in the run with $X_{ps}^{bulk} = 0.15$ at 0.5 GPa/600 °C only clinozoisite I overgrowths were

Table 2. Average composition of overgrowths as determined by electron microprobe. In parentheses standard deviations of the last decimals. In runs at 0.5 GPa, two clinozoisites with different compositions are present (see text); in runs at 2.0 GPa, only one clinozoisite formed

Run No.	T	Composition[a]	Zoisite overgrowth	Clinozoisite overgrowth (X_{ps}^{czo})	
	(°C)	(X_{ps}^{bulk})	(X_{ps}^{zo})	Clinozoisite I	Clinozoisite II
0.5 GPa					
AB 55	500	0.1	0.059 (8)	0.156 (15)	–
AB 58	500	0.25		0.26 (4)	–
AB 84	500	0.4	–	–	0.55 (3)
AB 88	500	0.6	–	–	0.60 (4)
AB 87	500	1.0	–	–	0.93 (5)
AB 74	550	0.125	0.058 (11)	0.158 (15)	–
AB 75	550	0.4	–	0.20 (5)	0.57 (5)
AB 76	550	0.6	–	–	0.61 (5)
AB 77	550	1.0	–	–	1.01 (4)
AB 95	575	0.125	0.068 (16)	0.181 (28)	–
AB 96	575	0.35	–	–	0.57 (7)
AB 49	600	0.1	0.079 (11)	0.20 (3)	–
AB 50	600	0.15	–	0.21 (2)	–
AB 51	600	0.2	–	0.21 (3)	–
AB 52	600	0.25	–	0.21 (2)	0.56 (4)
AB 91	600	0.6	–	–	0.70 (7)
AB 92	600	1.0	–	–	0.74 (7)
AB 78	650	0.45	0.112 (15)	–	–
AB 79	650	1.0	–	–	0.78 (6)
2.0 GPa					
AB P9	650	0.2	0.132 (12)	0.24 (1)	
AB P10	650	0.25	–	0.28 (2)	
AB P1	700	0.2	0.140 (14)	0.25 (3)	
AB P2	700	0.4	–	0.43 (4)	
AB P7	750	0.2	0.146 (12)	0.25 (1)	
AB P8	750	0.25	0.158 (11)	0.28 (1)	
AB P5	800	0.2	0.160 (12)	0.30 (4)	
AB P6	800	0.4	–	0.42 (2)	

[a]Composition on the join $Ca_2Al_3Si_3O_{11}(O/OH)$–$Ca_2Al_2Fe^{3+}Si_3O_{11}(O/OH)$ with 10 wt% excess SiO_2; $X_{ps} = Fe^{3+}/(Fe^{3+} + Al\text{-}2)$

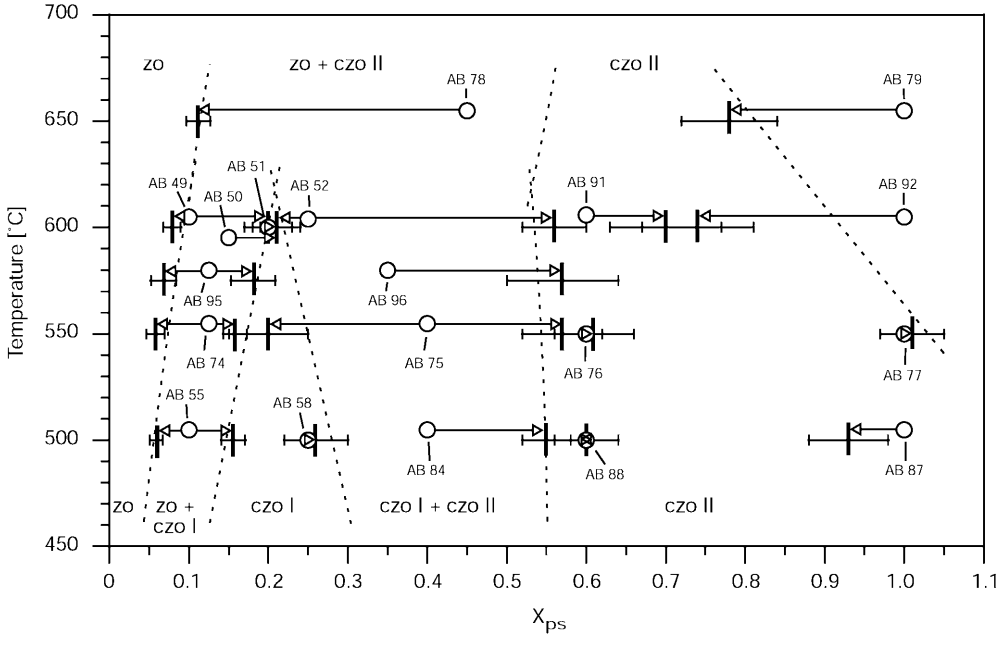

Fig. 3. Composition of zoisite and clinozoisite overgrowths from all runs at 0.5 GPa versus temperature (data from Table 2). *Vertical bars* denote average overgrowth composition (*error bars* represent standard deviation 1σ), *circles* denote bulk composition. *Arrows* connect each X_{ps}^{bulk} with the corresponding overgrowth. *Dashed lines* outline schematically the stability fields of zoisite (*zo*), clinozoisite I (*czo I*), and clinozoisite II (*czo II*). Zo + czo I, zo + czo II and czo I + czo II denote the corresponding two-phase fields (see text)

found with $X_{ps}^{overgrowth} > X_{ps}^{bulk}$ and $X_{ps}^{czoI} \sim 0.21$ (Table 2, Fig. 3). The run with $X_{ps}^{bulk} = 0.45$ at 0.5 GPa/650 °C yielded only zoisite overgrowths with $X_{ps}^{overgrowth} < X_{ps}^{bulk}$ and $X_{ps}^{zo} \sim 0.11$. The runs with $X_{ps}^{bulk} = 1.0$ at 0.5 GPa/500, 600 and 650 °C have only clinozoisite II overgrowths with $X_{ps}^{overgrowth} < X_{ps}^{bulk}$

(Table 2, Fig. 3). The runs with $X_{ps}^{bulk} = 0.6$ at 0.5 GPa/600 °C and $X_{ps}^{bulk} = 0.25$ at 2.0 GPa/650 °C yielded only clinozoisite overgrowths with $X_{ps}^{overgrowth}$ slightly higher than X_{ps}^{bulk} (Table 2, Figs. 3 and 4).

Discussion

Equilibrium conditions

For the evaluation of the experimental results it is most important to show that equilibrium was attained in our experimental set-up. The formation of clinozoisite pseudomorphs after zoisite seeds in runs AB 87, AB 77, AB 91, AB 92 and AB 79 clearly indicates decomposition of the zoisite seeds and reaction with the oxide–fluid mixture. Thus, the bulk compositions of these runs changed during the experiments and are not well constrained. Therefore, the results of these runs do not necessarily represent equilibrium conditions, although they are internally consistent and agree with results of previous studies (see below). In all other runs, we neither observe any resorption of the seed crystals nor did we find any significant diffusional exchange between seed crystals and overgrowths, indicating that in these runs a chemical exchange between seed and oxide–fluid mixture, if any, is negligible (Fig. 2). One might interpret the inner zones of the overgrowths as a result of a diffusion between seed crystal and overgrowth, but then we would not only expect an outward diffusion, as might be indicated by the inner zones, but also a diffusion into the seed crystals, which we did not observe. Another argument against an interpretation of the inner zones as diffusion zones are the zoisite overgrowths on zoisite seed crystals. In these cases, the inner zones have higher iron contents than the outer zones of the overgrowths (see Fig. 2a, d), which cannot be explained by diffusional exchange between seed and overgrowth. Therefore, we interpret the inner zones as representing the initial growth stages, most probably during heating of the experiments.

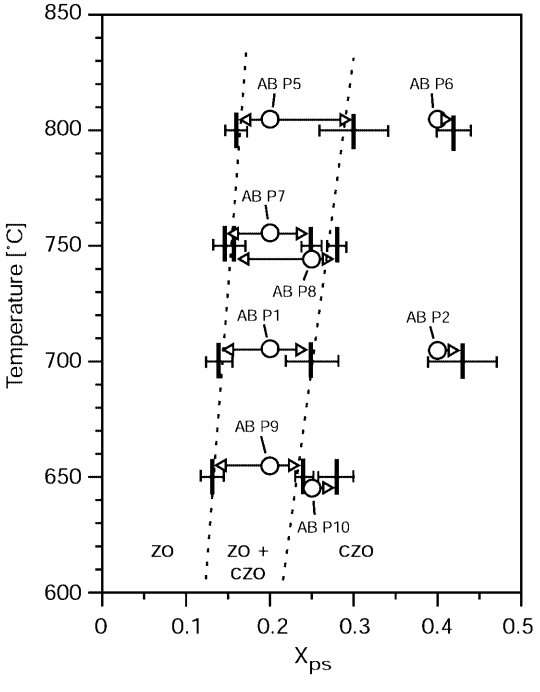

Fig. 4. Composition of zoisite and clinozoisite overgrowths from all runs at 2.0 GPa versus temperature (data from Table 2). *Vertical bars* denote average overgrowth composition (*error bars* represent standard deviation 1σ), *circles* bulk composition. *Arrows* connect each X_{ps}^{bulk} with the corresponding overgrowth. *Dashed lines* outline schematically the stability fields of zoisite (*zo*), clinozoisite (*czo*), and two-phase field zo + czo (see text)

It is also uncertain if the matrix assemblages represent equilibrium. The bulk compositions lie on the join $Ca_2Al_3Si_3O_{11}(O/OH)$–$Ca_2Al_2FeSi_3O_{11}(O/OH)$ with excess SiO_2. As long as this join is intact, one should expect two or three phase assemblages with quartz plus one or two epidote minerals, but Table 1 shows that the matrix assemblages typically consist of three or four phase assemblages with additional garnet and anorthite or hematite. In particular, the coexistence of anorthite and garnet in most of the 0.5-GPa runs indicates disequilibrium because, in the presence of quartz, the join $Ca_2Al_3Si_3O_{11}(O/OH)$–$Ca_2Al_2FeSi_3O_{11}(O/OH)$ separates anorthite-bearing assemblages from garnet-bearing assemblages, as can be seen in a CaO–Al_2O_3–Fe_2O_3 triangular plot (see Fig. 11a, b), and zoisite and clinozoisite should therefore either coexist with anorthite or with garnet. The reasons for this disequilibrium are most likely small heterogeneities of the charges because of incomplete homogenization, shifting the local bulk composition either to the anorthite or to the garnet side of the join $Ca_2Al_3Si_3O_{11}(O/OH)$–$Ca_2Al_2FeSi_3O_{11}(O/OH)$. Once anorthite or garnet formed, they persist metastably. But the disequilibria of the matrix assemblages have no effects on the derived zoisite–clinozoisite phase equilibria because, for a given P and T, the compositions of coexisting zoisite + clinozoisite or clinozoisite I + clinozoisite II are fixed, regardless if they coexist with anorthite or with garnet.

Another point, which must be addressed, is the validity of designating ΣFe as Fe^{3+}. It is unlikely that significant amounts of Fe^{2+} formed during the runs because in runs with $X_{ps}^{bulk} = 1.0$ only hematite was observed as a product phase, but no Fe^{2+}-oxides (e.g. magnetite). If small amounts of Fe^{2+} were present in the runs, they would enter into garnet [$(Ca,Fe^{2+})_3(Al,Fe^{3+})_2Si_3O_{12}$], the only phase in this simplified synthetic system that might incorporate Fe^{2+}, and neither into zoisite nor clinozoisite. Small amounts of Fe^{2+}, therefore, have no effects on the zoisite–clinozoisite phase equilibria.

The most important point, however, is to demonstrate, that the outer zones of the overgrowths represent equilibrium compositions because our interpretation and the derived zoisite–clinozoisite phase equilibria are almost exclusively based on the composition of these overgrowths. Although the inner zones of the over-

growths are inhomogeneous (Fig. 2) and might represent disequilibrium during the initial growth stages, we have good evidence for equilibration during the growth of the outer zones. Firstly, not only are the outer zones of each individual overgrowth homogeneous, but the composition of all the individual zoisite or clinozoisite overgrowths of one experiment is homogeneous as well. Secondly, the results of all runs yield an internally consistent data set of zoisite–clinozoisite phase relations, such as increasing X_{ps} in coexisting zoisite and clinozoisite with increasing temperature at both pressures (Figs. 3 and 4) or consistent X_{ps}^{czoII} in runs AB 84, AB 75, AB 96 and AB 52 at 0.5 GPa (Fig. 3). Thirdly, the composition of clinozoisite I in the runs with $X_{ps}^{bulk} = 0.1$ and 0.15 at 0.5 GPa/600 °C is consistently independent of X_{ps}^{bulk}. The same is valid for the zoisite and clinozoisite overgrowths in the runs with $X_{ps}^{bulk} = 0.2$ and 0.25 at 2.0 GPa/750 °C.

In summary, although we are not able to demonstrate unequivocally, we have good evidence that the outer zones of the overgrowths represent equilibrium compositions, and that the derived zoisite–clinozoisite phase relations represent phase equilibria. Regarding the join $Ca_2Al_3Si_3O_{11}(O/OH)$–$Ca_2Al_2FeSi_3O_{11}(O/OH)$, this means that the compositions of coexisting zoisite + clinozoisite and clinozoisite I + clinozoisite II (cases a and b, see above), define the limbs of the corresponding two-phase fields, whereas runs, in which $X_{ps}^{overgrowth} \sim X_{ps}^{bulk}$ (case c, see above), define one-phase fields. The results, therefore, show us that there are no continuous solid solutions between either zoisite and clinozoisite or within the monoclinic solid solution series at run conditions.

Some problems arise from those runs in which only one kind of overgrowth was found that deviates in composition from X_{ps}^{bulk} (case d, see above). The bulk composition of runs AB 84 and AB 96 falls inside the 'czo I + czo II' two-phase field, whereas that of run AB 50 falls inside the 'zo + czo I' two-phase field (Fig. 3). The runs AB 84 and AB 96, therefore, should show coexisting clinozoisite I and II overgrowths and run AB 50 should show coexisting zoisite and clinozoisite I overgrowths. The lack of clinozoisite I overgrowths in runs AB 84 and AB 96 and zoisite overgrowths in AB 50 is probably because of our preparation procedure because we were neither able to distinguish between different overgrowths before sample preparation nor to properly orient the embedded seed crystals, thus it was always a question of fortune to find the appropriate well-prepared overgrowths. The same is probably true for the lack of clinozoisite II overgrowths in run AB 78, where the bulk composition falls inside the 'zo + czo II' two-phase field (Fig. 3). The chemical shift in runs AB 92 and AB 79 (Fig. 3) is balanced by the precipitation of hematite and represents the upper thermal stability of iron-rich clinozoisite II (see below). The chemical shift in runs AB 87, AB 91 and AB P10 (Figs. 3 and 4) is only minor and might be caused by co-precipitation of garnet and/or hematite, or the formation of pseudomorphs that shift the bulk composition of the runs either to iron-richer or iron-poorer compositions.

Zoisite–clinozoisite phase relations

To explore the two-phase field between zoisite and clinozoisite, we used only the results of those runs in which zoisite and clinozoisite overgrowths coexist and, therefore, that define the limbs of the zoisite–clinozoisite two-phase field (Table 2, Fig. 5). At both pressures, this two-phase field is relatively narrow and would extend with increasing iron content to very high temperatures (Fig. 5), well above the upper thermal stabilities of zoisite and clinozoisite. Because we did not find coexisting clinozoisite I and II in any of the 2.0-GPa runs, we have no proof if the clinozoisite overgrowths at 2.0 GPa represent clinozoisite I or II. But the similarities in the 'zo + czo' two-phase fields at 0.5 and 2.0 GPa and especially the linear relationship in a ln $K_{D,red}$ vs. 1/T plot (Fig. 6) strongly suggest that the clinozoisite overgrowths at 2.0 GPa are clinozoisite I and, therefore, can be combined with the results at 0.5 GPa.

Tentative linear fits to the zoisite and clinozoisite limbs at 0.5 GPa (Fig. 5a) and 2.0 GPa (Fig. 5b), result in the expressions for the maximum and minimum iron contents in coexisting zoisite and clinozoisite I as functions of T at both pressures. Combining these expressions for $X_{ps}^{zo}(max)$ and $X_{ps}^{czo}(min)$ at 0.5 and 2.0 GPa, and assuming a linear pressure dependence, yields the expressions for the maximum and minimum iron contents in coexisting zoisite and clinozoisite I as functions of P and T (with P in GPa and T in °C):

$$X_{ps}^{zo}(max) = 1.9 * 10^{-4}T + 3.1 * 10^{-2}P - 5.63 * 10^{-2} \quad (1)$$

$$X_{ps}^{czoI}(min) = (4.6 * 10^{-4} - 4 * 10^{-5}P)T + 3.82 * 10^{-2}P - 8.76 * 10^{-2}. \quad (2)$$

Equation (1) indicates that a temperature or pressure increase of $\Delta T \sim 50$ °C or $\Delta P \sim 0.3$ GPa increases $X_{ps}^{zo}(max)$ by 0.01. Figure 7a shows lines of constant $X_{ps}^{zo}(max)$ calculated with Eq. (1) dependent on P and T. In contrast to zoisite, Eq. (2) shows that in clinozoisite I, a temperature increase of $\Delta T = 50$ °C increases $X_{ps}^{czoI}(min)$ by 0.02. The influence of pressure on $X_{ps}^{czoI}(min)$ depends largely on the temperature: at T = 500 °C a pressure increase of $\Delta P \sim 0.5$ GPa increases $X_{ps}^{czoI}(min)$ by 0.01, whereas at T = 800 °C a much higher pressure increase of $\Delta P \sim 1.6$ GPa is necessary to yield the same effect on $X_{ps}^{czoI}(min)$.

Extrapolation of the zoisite and clinozoisite limbs to lower X_{ps} values yields temperatures for the iron-free end members of T = 215 °C (zo-limb) and 156 °C (czo I-limb) at 0.5 GPa (Fig. 5a) and T = –30 °C (zo-limb) and 30 °C (czo I-limb) at 2.0 GPa (Fig. 5b). Because of the scatter of the experimental results and our simplified linear fit, the errors in the derived temperatures are definitely large, nevertheless the data suggest equilibrium temperatures for the iron-free end member reaction

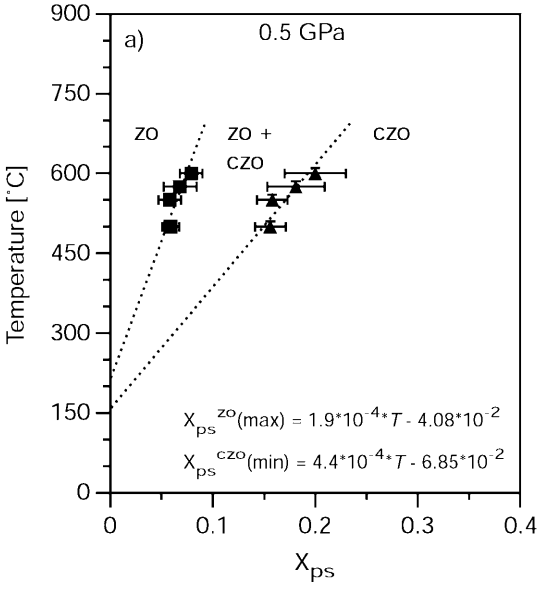

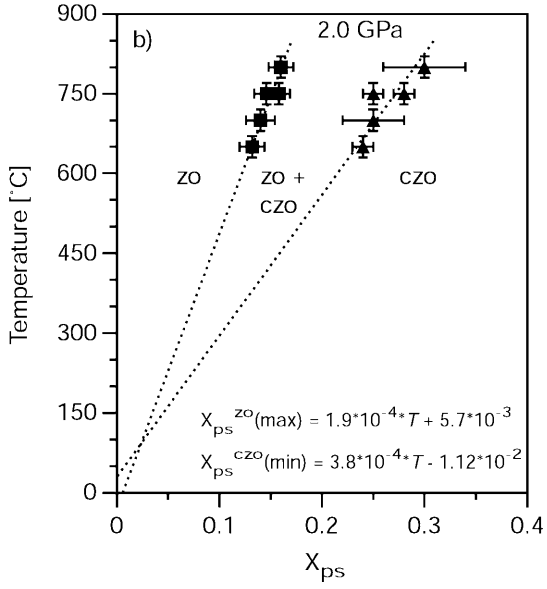

Fig. 5a, b. Composition of coexisting zoisite and clinozoisite overgrowths at **a** 0.5 GPa and **b** 2.0 GPa. The limbs of the zo + czo two-phase fields are tentatively extrapolated to lower X_{ps} as *straight lines*. Equations show the temperature dependence of maximum and minimum X_{ps} in coexisting zoisite and clinozoisite. *czo* Clinozoisite; *zo* zoisite

clinozoisite I = zoisite (3)

of $T_{eq} = 185 \pm 50$ °C at 0.5 GPa and $T_{eq} = 0 \pm 50$ °C at 2.0 GPa. This indicates that reaction (3) has a negative slope of ~–8 MPa/ °C.

An equilibrium temperature of ~185 °C at 0.5 GPa for reaction (3) agrees well with the data presented by Jenkins et al. (1983, 1985). They found that clinozoisite is stable at $T < 200$ °C. Also, the equilibrium temperature given by Franz and Selverstone (1992) for low to intermediate pressure conditions of $T_{eq} = 160$ °C is in accordance with our estimate for 0.5 GPa, and their proposal that, at high pressure, this temperature must lie significantly below 100 °C agrees with $T_{eq} = 0 \pm 50$ °C/ 2.0 GPa (Fig. 5b) as determined here. In contrast, Holdaway (1972) determined $T_{eq} = 635 \pm 75$ °C and Holland (1984) determined $T_{eq} = 500 \pm 25$ °C; the reasons for these discrepancies are not clear. A low equilibrium temperature for reaction (3) is also supported by natural assemblages, where iron-poor clinozoisite is described (Deer et al. 1986).

In order to evaluate quantitatively the influence of iron on reaction (3), data for ΔV, ΔH_r^0 and ΔS_r^0 of reaction (3) at standard conditions (298 K and 0.1 MPa) are required. At equilibrium

$$\Delta G_r = 0 = \Delta H_r^0 + \int_{298}^{T} \Delta C_p dT + \int_{0.1}^{P} \Delta V dP - T\left(\Delta S_r^0 + \int_{298}^{T} \frac{\Delta C_p}{T} dT\right) + RT \ln K \quad (4)$$

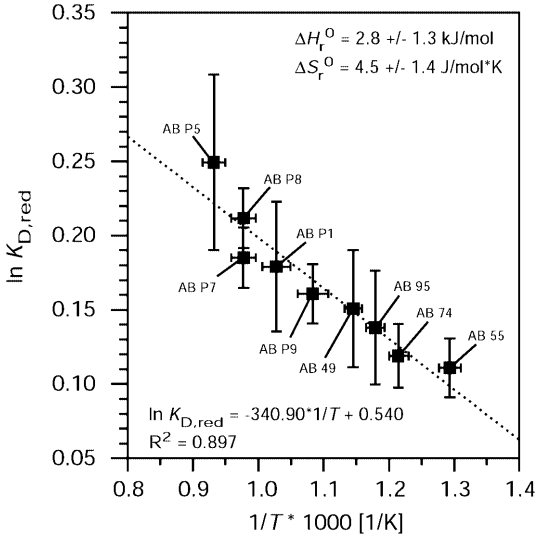

Fig. 6. ln $K_{D,red}$ vs. $1/T$ plot for reaction (3) clinozoisite = zoisite, as determined for the experimental conditions between 500 and 800 °C at 0.5 and 2.0 GPa. The regression line yields $\Delta H_r^0 = 2.8 \pm 1.3$ kJ/mol and $\Delta S_r^0 = 4.5 \pm 1.4$ J/mol × K (see text for calculation of ln $K_{D,red}$)

must be valid. Following Prunier and Hewitt (1985) and taking

$$K = \frac{a_{Al}^{zo}}{a_{Al}^{czoI}} = \frac{x_{Al}^{zo}\gamma_{Al}^{zo}}{x_{Al}^{czoI}\gamma_{Al}^{czoI}}, \quad (5)$$

$$x_{Al}^{zo} = 1 - x_{ps}^{zo}, \quad (6)$$

$$x_{Al}^{czoI} = 1 - x_{ps}^{czoI}, \text{and} \quad (7)$$

$$K_D = \frac{1 - x_{ps}^{zo}}{1 - x_{ps}^{czoI}}, \quad (8)$$

with subscript 'Al' denoting the Al end members in the respective solid solutions, one arrives at

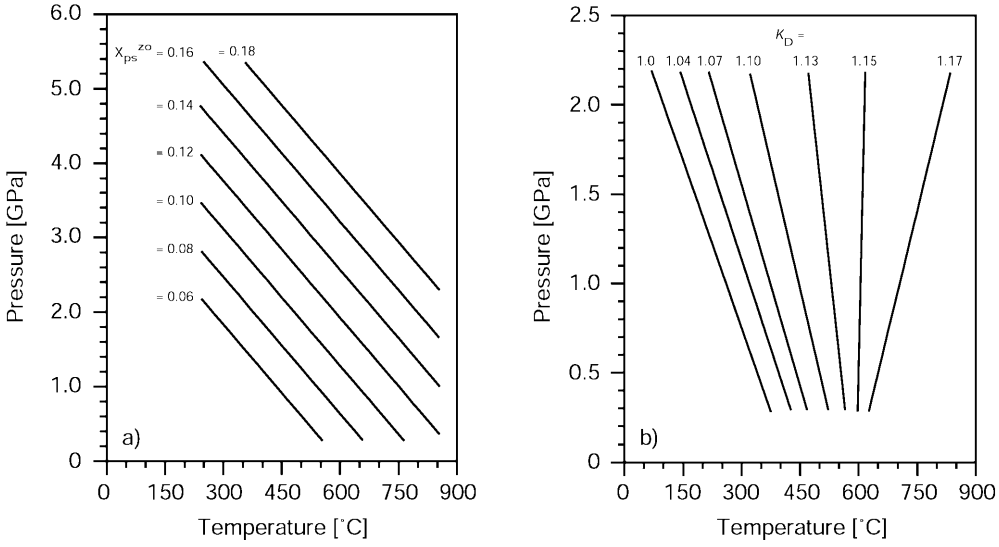

Fig. 7. **a** Lines of constant zoisite composition as a function of P and T, indicating the minimum P–T conditions for the respective iron content. **b** Iso-K_D-lines for the reaction (3) clinozoisite = zoisite in P–T field. Increasing K_D indicates increasing Fe content in clinozoisite and zoisite. The slopes are fairly steep and change from negative to positive with increasing K_D

$$\Delta G_r = 0 = \Delta H_r^0 + \int_{298}^{T} \Delta C_p dT + \int_{0.1}^{P} \Delta V dP - T\left(\Delta S_r^0 + \int_{298}^{T} \frac{\Delta C_p}{T} dT\right) + RT \ln \frac{\gamma_{Al}^{zo}}{\gamma_{Al}^{czoI}} + RT \ln K_D. \quad (9)$$

The thermodynamic databases of Berman and Brown (1985) and Hemingway et al. (1982) each report identical C_p functions for zoisite and clinozoisite, indicating that C_p may be very similar for zoisite and clinozoisite. There exist no data for $\gamma_{Al}{}^{zo}$ and $\gamma_{Al}{}^{czoI}$. For the considered zoisite and clinozoisite overgrowths with low iron contents, we suggest that $\gamma_{Al}{}^{zo}$ and $\gamma_{Al}{}^{czoI}$ are more or less similar. The errors introduced by the simplifications $\Delta C_p = 0$ and $\gamma_{Al}{}^{zo}/\gamma_{Al}{}^{czoI} = 1$, therefore, are expected to be small, and hence the Eq. (9) may be simplified to

$$\Delta G_r = 0 = \Delta H_r^0 - T\Delta S_r^0 + \int_{0.1}^{P} \Delta V dP + RT \ln K_D. \quad (10)$$

The last two terms of Eq. (10) can be combined to the reduced distribution coefficient $K_{D,red}$ with

$$RT \ln K_{D,red} = \int_{0.1}^{P} \Delta V dP + RT \ln K_D, \quad (11)$$

which leads to

$$\Delta G_r = 0 = \Delta H_r^0 - T\Delta S_r^0 + RT \ln K_{D,red}, \text{ or} \quad (12)$$

$$\ln K_{D,red} = -\frac{\Delta H_r^0}{R} * \frac{1}{T} + \frac{\Delta S_r^0}{R}. \quad (13)$$

The volume integral for reaction (3) at P and T may be expressed as (Gottschalk 1997)

$$\int_{0.1}^{P} \Delta V dP = \left[\frac{V_{zo}^0}{\beta_{zo}^0} e^{\alpha_{zo}^0 (T-298)} \left(1 - e^{-\beta_{zo}^0 (P-0.1)}\right)\right] - \left[\frac{V_{czoI}^0}{\beta_{czoI}^0} e^{\alpha_{czoI}^0 (T-298)} \left(1 - e^{-\beta_{czoI}^0 (P-0.1)}\right)\right]. \quad (14)$$

We calculated $K_{D,red}$ for each run, in which zoisite and clinozoisite I overgrowths coexist, taking $V_{zo}{}^0 = 135.74$ J/MPa × mol and $V_{czoI}{}^0 = 136.27$ J/MPa × mol (Brunsmann 2000), $\beta_{zo}{}^0 = 8.77 \times 10^{-6}$ MPa^{-1} and $\beta_{czoI}{}^0 = 7.69 \times 10^{-6}$ MPa^{-1} (Comodi and Zanazzi 1997) and $\alpha_{zo}{}^0 = 3.86 \times 10^{-5}$ K^{-1} and $\alpha_{czoI}{}^0 = 2.94 \times 10^{-5}$ K^{-1} (Pawley et al. 1996). The plot of the data in a ln $K_{D,red}$ vs. 1/T diagram (Fig. 6) points out a linear relation, as expected, with a slope of $-\Delta H_r{}^0/R$ and an intercept of $\Delta S_r{}^0/R$. A linear fit to the data yields $\Delta H_r{}^0 = 2.8 \pm 1.3$ kJ/mol and $\Delta S_r{}^0 = 4.5 \pm 1.4$ J/mol × K. These values agree well with published data (Table 3); they demonstrate the only small energetic difference between zoisite and clinozoisite I and are comparable in magnitude with those of other transformations, e.g. between the aluminosilicates sillimanite, kyanite and andalusite or between aragonite and calcite (Gottschalk 1997). $\Delta H_r{}^0$ and $\Delta S_r{}^0$

Table 3. Values of $\Delta H_r{}^0$ and $\Delta S_r{}^0$ of the iron-free end member reaction clinozoisite = zoisite from this study and the literature

Source	$\Delta H_r{}^0$ (kJ/mol)	$\Delta S_r{}^0$ (J/K × mol)
This study	2.8 ± 1.3	4.5 ± 1.4
Berman (1988)	5.48	10.5
Gottschalk (1997)	3.63 ± 1.80	10.7 ± 0.6
Helgeson et al. (1978)	0.377	0.418
Holland and Powell (1990)	4.81 ± 13.08	4
Jenkins et al. (1985)	4.5	9.35

were then used to calculate lines of constant K_D in P–T space for reaction (3) according to Eq. (10) and (14). The slope of these lines is fairly steep and changes from negative to positive values with increasing K_D ($K_D = 1.0$: $dP/dT = -6.3$ MPa/K, $K_D = 1.17$: $dP/dT = 0.11$ MPa/K) as shown in Fig. 7b.

Solid solution in clinozoisite

The runs with $X_{ps}^{bulk} = 0.4$ and $X_{ps}^{bulk} = 0.25$ at 0.5 GPa/550 and 600 °C yielded coexisting clinozoisite I and II and clearly show that, at least at 0.5 GPa, the clinozoisite solid solution series exhibits a miscibility gap in the range of X_{ps} ~0.25–0.5. Our results suggest that at 0.5 GPa this miscibility gap widens with increasing temperature (Fig. 3). The maximum iron content in clinozoisite I decreases with increasing temperature from $X_{ps}^{czoI}(max) > 0.26 \pm 0.04$ at 500 °C to $X_{ps}^{czoI}(max) = 0.21 \pm 0.02$ at 600 °C, whereas the minimum iron content in clinozoisite II is $X_{ps}^{czoII}(min)$ ~0.55 independent of temperature (Table 2, Fig. 3). With increasing temperature $X_{ps}^{czoI}(min)$ increases (see above) whereas $X_{ps}^{czoI}(max)$ decreases and the stability field of clinozoisite I consequently narrows with increasing temperature (Fig. 3). At a temperature slightly above 600 °C, the 'zo + czo I' and 'czo I + czo II' two-phase fields intersect and clinozoisite I disappears (Fig. 3). This is consistent with the run at 650 °C/$X_{ps}^{bulk} = 0.45$, in which large homogeneous zoisite overgrowths formed (Figs. 1e and 3). If clinozoisite I is still stable at this temperature, one would expect clinozoisite I overgrowths instead of zoisite overgrowths.

Heuss-Aßbichler and Fehr (1997) and Fehr and Heuss-Aßbichler (1997) found a similar gap in their experimental study at 0.3 GPa, and postulated a metastable critical temperature of the solvus of 730 °C and a breakdown of the Al-rich clinozoisite (identical to clinozoisite I of this study) at T < 650 °C according to the reaction

$$\text{clinozoisite} = \text{anorthite} + \text{garnet} + \text{hematite}, \quad (15)$$

but did not consider the intersection of the miscibility gap with the 'zo–czo' two-phase loop. The upper thermal stability of clinozoisite I, therefore, is given by the reaction

$$\text{clinozoisite I} = \text{zoisite} + \text{clinozoisite II}. \quad (16)$$

According to Heuss-Aßbichler and Fehr (1997) and Fehr and Heuss-Aßbichler (1997) the reason for the 'czo I + czo II' two-phase field are ordering phenomena of Al and Fe^{3+} on the M3 site in clinozoisite.

No detailed attempt was made to determine the possible existence of miscibility gaps at 0.5 GPa and iron contents of $X_{ps} > 0.55$, although our results put some limits on such miscibility gaps. At 500 °C/$X_{ps}^{bulk} = 0.6$ and 550 °C/$X_{ps}^{bulk} = 0.6$ large homogeneous clinozoisite II overgrowths were synthesized on the bulk compositions (Table 2, Fig. 3). At these temperatures a potential miscibility gap must be located at $X_{ps} > 0.6$. At 600 °C/$X_{ps}^{bulk} = 0.6$ and 1.0, clinozoisite II overgrowths formed with $X_{ps}^{czoII} = 0.70 \pm 0.07$ and 0.74 ± 0.07, which indicates that in the compositional range X_{ps} ~0.6–0.8, the critical temperature of a potential miscibility gap must be < 600 °C.

Upper thermal stability of Fe-rich clinozoisite at 0.5 GPa

The results of the runs with $X_{ps}^{bulk} = 1.0$ at 550, 600 and 650 °C give some information about the upper thermal stability of what is generally known as the iron end member $Ca_2Al_2FeSi_3O_{11}(O/OH)$ of the clinozoisite solid solution series. More than $X_{ps}^{czo} = 1.0$ in clinozoisite is rarely reported and, in most cases where $X_{ps}^{czo} > 1.0$, the minerals were formed at very low temperatures in hydrothermal fields and are considered to be metastably disordered (e.g. Bird et al. 1988). The clinozoisite II overgrowths with $X_{ps}^{czoII} = 1.01 \pm 0.04$ at 550 °C indicate that the iron end member is stable at this temperature whereas the clinozoisite II overgrowths with $X_{ps}^{czoII} = 0.74 \pm 0.07$ at 600 °C and 0.78 ± 0.06 at 650 °C indicate that it is unstable at temperatures above 550 °C. This is in agreement with data of Heuss-Aßbichler and Fehr (1997), who determined maximum iron contents in clinozoisite of $X_{ps}^{czo} = 0.96$ at 0.3 GPa/600 °C and $X_{ps}^{czo} = 0.88$ at 0.3 GPa/650 °C. Their slightly higher values might be explained by the lower pressure of their study.

The formation of hematite in runs AB 92 and AB 79 and the decreasing maximum iron content in clinozoisite II with increasing temperature is consistent with the breakdown of clinozoisite II with increasing temperature according to the sliding reaction (in the presence of quartz and water)

$$\text{Fe-rich clinozoisite II} = \text{Fe-poor clinozoisite II} + \text{garnet} + \text{hematite}, \quad (17)$$

that was already proposed by Liou et al. (1983).

Conclusions

The zoisite–clinozoisite equilibrium

The major characteristics of the two-phase loop as determined here are in good agreement with the previous hypotheses of Raith (1976), Enami and Banno (1980) Prunier and Hewitt (1985) and Franz and Selverstone (1992). Zoisite is the iron-poor high-temperature form, clinozoisite the iron-rich low-temperature form. Coexisting zoisite and clinozoisite become more enriched in iron with increasing temperature. However, the dimensions of the two-phase loop as determined here are significantly different than in the aforementioned studies. Also, the iron content in clinozoisite, as determined here,

is much lower than those observed in natural assemblages.

A possible explanation for this phenomenon is that in the studies of the natural occurrences the ascribed P–T conditions are uncertain and, therefore, the error in locating the position of the two-phase loop is relatively large. Raith (1976) and Enami and Banno (1980) did not consider the qualitative influence of pressure. Also, clinozoisite can be strongly zoned, generally to a much greater degree than the coexisting zoisite, and it remains uncertain which composition was in equilibrium during peak metamorphic conditions. Franz and Selverstone (1992) assumed for their high-pressure assemblages that the rims of zoned clinozoisites with $X_{ps} = 0.43$–0.48 were in equilibrium with coexisting zoisite. Using their values for the core composition of the clinozoisites ($X_{ps} = 0.3$–0.35), the agreement with our experimental determination at 2.0 GPa is much better. The experimental determination of Prunier and Hewitt (1985) at 650 °C and 0.65 GPa yielded $X_{ps}^{czo} = 0.57$, which is in good agreement with our observations, because clinozoisite I did not form at temperatures above 600 °C and the composition of $X_{ps}^{czo} = 0.57$ fits our data for clinozoisite II accurately (Fig. 3). However, Prunier and Hewitt (1985) found $X_{ps}^{zo} = 0.18$ in the coexisting zoisite, which is much higher than what was observed here. Instead, this zoisite composition determined by Prunier and Hewitt (1985) would correspond to clinozoisite I.

The use of the zoisite–clinozoisite phase equilibrium as a geothermobarometer

Although suggested by the steep slope of the lines of constant K_D in Fig. 7b, the zoisite–clinozoisite phase equilibrium is not a suitable geothermometer. Because of the very narrow 'zo + czo I' two-phase field, the changes of K_D with temperature are only minor and an increase in K_D of only 0.17 spans the whole relevant temperature conditions (Fig. 7b). If we assume that X_{ps}^{zo} and X_{ps}^{czo} can be determined with a precision of $\Delta X_{ps} \sim \pm 0.01$, then K_D can be determined with $\Delta K_D \sim \pm 0.03$. As Fig. 7b indicates, such an error in K_D corresponds to a large error in the derived temperature of $\Delta T > \pm 100$ °C. In contrast, the maximum iron contents in zoisite are well constrained in our experiments and, therefore, can be used to calculate approximate minimum P–T conditions, even in rocks that lack clinozoisite. However, according to Eq. (1) and Fig. 7a, an error in X_{ps}^{zo} of $\Delta X_{ps} = \pm 0.01$ still results in an error in T(min) and P(min) of $\Delta T = \pm 50$ °C and $\Delta P = \pm 0.3$ GPa. Nevertheless, an error of $\Delta P = \pm 0.3$ GPa is very acceptable for zoisite from high pressure rocks.

The influence of iron on the stability field of zoisite

Our data allowed us to qualitatively evaluate the influence of iron on the stability field of zoisite. At intermediate pressure, the upper thermal stability of iron-free zoisite is given by the subsolidus reactions (Fig. 8)

$$\text{zoisite} + \text{quartz} = \text{anorthite} + \text{grossular} + H_2O \quad (18)$$

$$\text{zoisite} = \text{anorthite} + \text{grossular} + \text{corundum} + H_2O \quad (19)$$

as determined previously by Winkler and Nitsch (1962), Newton (1965, 1966), Boettcher (1970) and Chatterjee et al. (1984). At high pressure, the stability field of iron-free zoisite is limited by the reactions

$$\text{zoisite} + \text{coesite} + H_2O = \text{lawsonite} + \text{grossular} \quad (20)$$

$$\text{zoisite} + H_2O = \text{kyanite} + \text{lawsonite} + \text{grossular} \quad (21)$$

$$\text{zoisite} = \text{kyanite} + \text{coesite} + \text{lawsonite} + \text{grossular} \quad (22)$$

$$\text{zoisite} = \text{kyanite} + \text{coesite} + \text{grossular} + H_2O \quad (23)$$

$$\text{zoisite} + \text{kyanite} + \text{coesite} + H_2O = \text{melt} \quad (24)$$

(Fig. 9, Schmidt and Poli 1994; Poli and Schmidt 1998). Assuming that the iron incorporation in anorthite, kyanite and lawsonite is negligible, the influence of Fe^{3+}

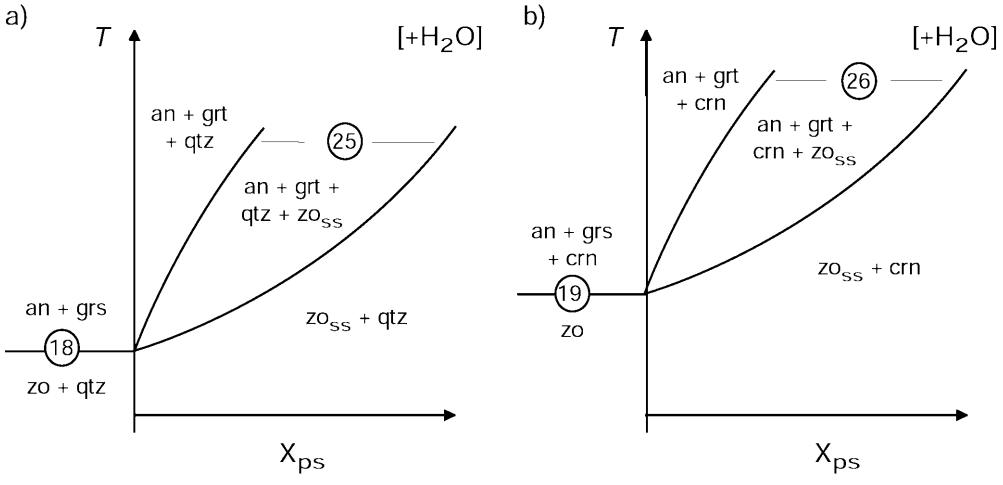

Fig. 8. Schematic T–X_{ps} diagram for the upper thermal stability of zoisite solid solution (zo_{ss}) with **a** quartz and **b** without quartz. In the iron-bearing system, the stability of zoisite is shifted to higher temperatures (*numbers* refer to reactions mentioned in the text. *an* Anorthite; *crn* corundum; *grs* grossular; *grt* garnet; *qtz* quartz; *zo* zoisite; $_{ss}$ solid solution)

on the position of these univariant equilibria in the P–T field depends exclusively on the distribution of Fe^{3+} between zoisite and garnet. Although in our run products garnet could not be analysed by electron microprobe because the grains were too small for reliable measurements, our results suggest a preferred iron incorporation in zoisite compared with garnet and an enlarged zoisite stability field in the iron-bearing system. At 0.5 GPa, the equilibrium temperature for reaction (18) is 620 ± 10 °C (Newton 1965, 1966; Boettcher 1970; Chatterjee et al. 1984). Our runs with $X_{ps}^{bulk} = 0.0$ at 0.5 GPa/600 and 650 °C are consistent with this temperature because no zoisite overgrowths formed and the matrix is only anorthite, grossular and quartz (at 650 °C). In contrast, our run with $X_{ps}^{bulk} = 0.45$ at 0.5 GPa/650 °C, approximately 30 °C above the upper thermal stability of iron-free zoisite, yielded large homogeneous zoisite overgrowths. This implies that iron increases the upper thermal stability of zoisite and that with increasing temperature zoisite solid solutions break down according to the sliding reactions

$$\text{Fe-poor zoisite} + \text{quartz} = \text{Fe-rich zoisite} + \text{anorthite} + \text{garnet} + H_2O \text{ and} \quad (25)$$

$$\text{Fe-poor zoisite} = \text{Fe-rich zoisite} + \text{anorthite} + \text{garnet} + \text{corundum} + H_2O \quad (26)$$

as shown schematically in Fig. 8. Our run with $X_{ps}^{bulk} = 0.2$ at 2.0 GPa/800 °C further supports an enlarged zoisite stability field in the iron-bearing system. According to Poli and Schmidt (1998), reaction (24) has an equilibrium temperature of 770 °C at 2.0 GPa, and according to Boettcher (1970) the reaction

$$\text{zoisite} + \text{quartz} + H_2O = \text{grossular} + \text{melt} \quad (27)$$

has an equilibrium temperature of 810 °C at 2.0 GPa. If iron reduces the stability field of zoisite, the run with $X_{ps}^{bulk} = 0.2$ at 2.0 GPa/800 °C should have produced melt, but it yielded large homogeneous zoisite overgrowths instead (Figs. 1d and 2d).

The principal effects of iron on the stability field of zoisite at high pressure are shown schematically in Fig. 9. Our data suggest that iron stabilizes zoisite at the expense of garnet and/or melt and, therefore, reactions (20), (21) and (22) will shift to lower temperatures, reaction (23) to higher pressures, and reactions (24) and (25) to higher temperatures; the stability field of zoisite, which is relatively small in the iron-free system, might significantly increase in the iron-bearing system. This has an important consequence for subduction zone environments: lawsonite will break down at a lower temperature compared with the iron-free system, and zoisite, which might contain very high concentrations of trace elements such as Pb, Sr and the rare earth elements (Brastad 1985; Nagasaki and Enami 1998; Brunsmann et al. 2000), will become a modally important phase in such rocks, controlling the distribution of these trace elements between fluids and solids.

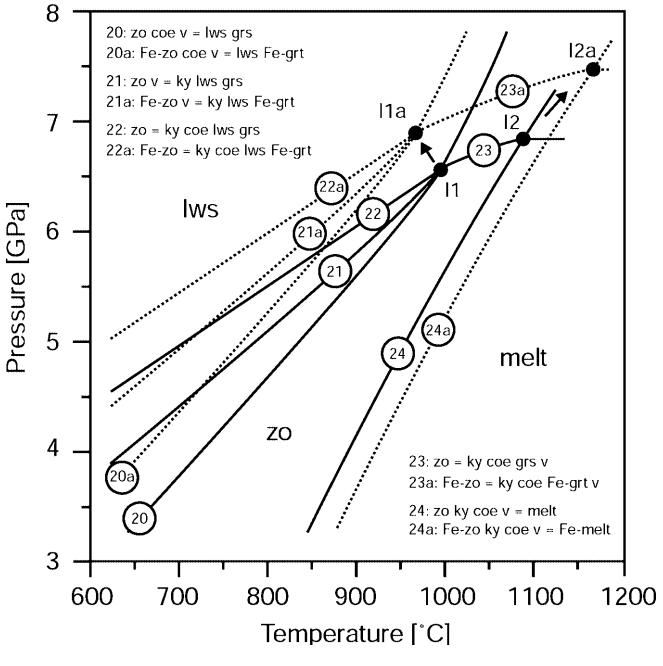

Fig. 9. P–T diagram, showing the high-pressure stability limits of zoisite in the pure system $CaO–Al_2O_3–SiO_2–H_2O$ (*straight lines*) and the qualitative influence of adding iron to the system (*dotted lines*). Incorporation of iron enlarges the stability field of zoisite (redrawn after Poli and Schmidt 1998; *numbers* refer to reactions mentioned in the text. *coe* Coesite; *grs* grossular; *grt* garnet; *lws* lawsonite; *ky* kyanite; *v* volatile; *zo* zoisite)

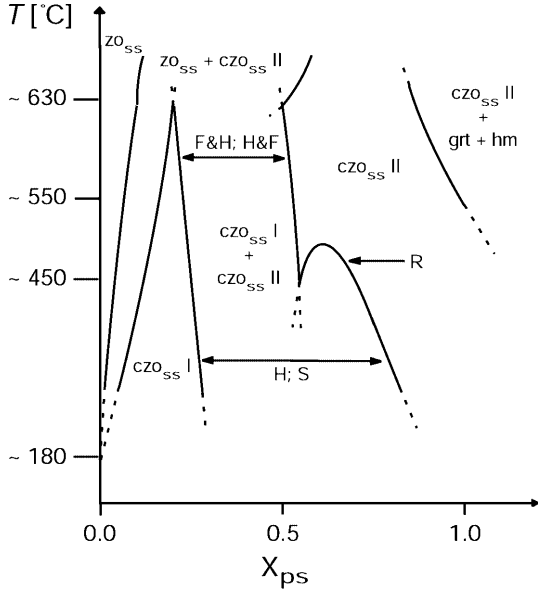

Fig. 10. Schematic T–X_{ps} diagram for the epidote minerals at intermediate pressure, as derived from experimental work (this study, *F&H* Fehr and Heus-Aßbichler 1997; *H&F* Heus-Aßbichler and Fehr 1997) and from studies on natural assemblages (*H* Hietanen 1974; *R* Raith 1976; *S* Strens 1963, 1964. *czo* Clinozoisite; *grt* garnet; *hm* hematite; *zo* zoisite; *ss* solid solution)

The problem of clinozoisite miscibility gaps

A combination of our results with those of previous studies yields a schematic picture of the phase relations among zoisite and clinozoisite at intermediate pressure (Fig. 10). There is a miscibility gap in the monoclinic solid solution series at low iron contents between approximately $X_{ps}^{czo} \sim 0.25$ and 0.5. Our data indicate that this gap does not close with increasing temperature. In natural rocks, Selverstone and Spear (1985) found a similarly wide miscibility gap, but they speculated that it should close at a temperature of 450 °C. In this context we want to emphasize that the effect of pressure on the location of the solvus is unknown. Moreover, the influence of minor elements such as Sr, Mn, Cr and rare earth elements, which may reach a few percent in zoisite and clinozoisite, may be significant for phase relations and phase transitions. Contrary to the results of this study, the early works of Strens (1963, 1964) and Hietanen (1974), which are based on natural mineral assemblages and empirical estimates of temperature of formation, show a much wider miscibility gap with the limb of the iron-rich part of the solvus at approximately $X_{ps} = 0.7$–0.8 (Fig. 10). An intersection of the 'czo I +

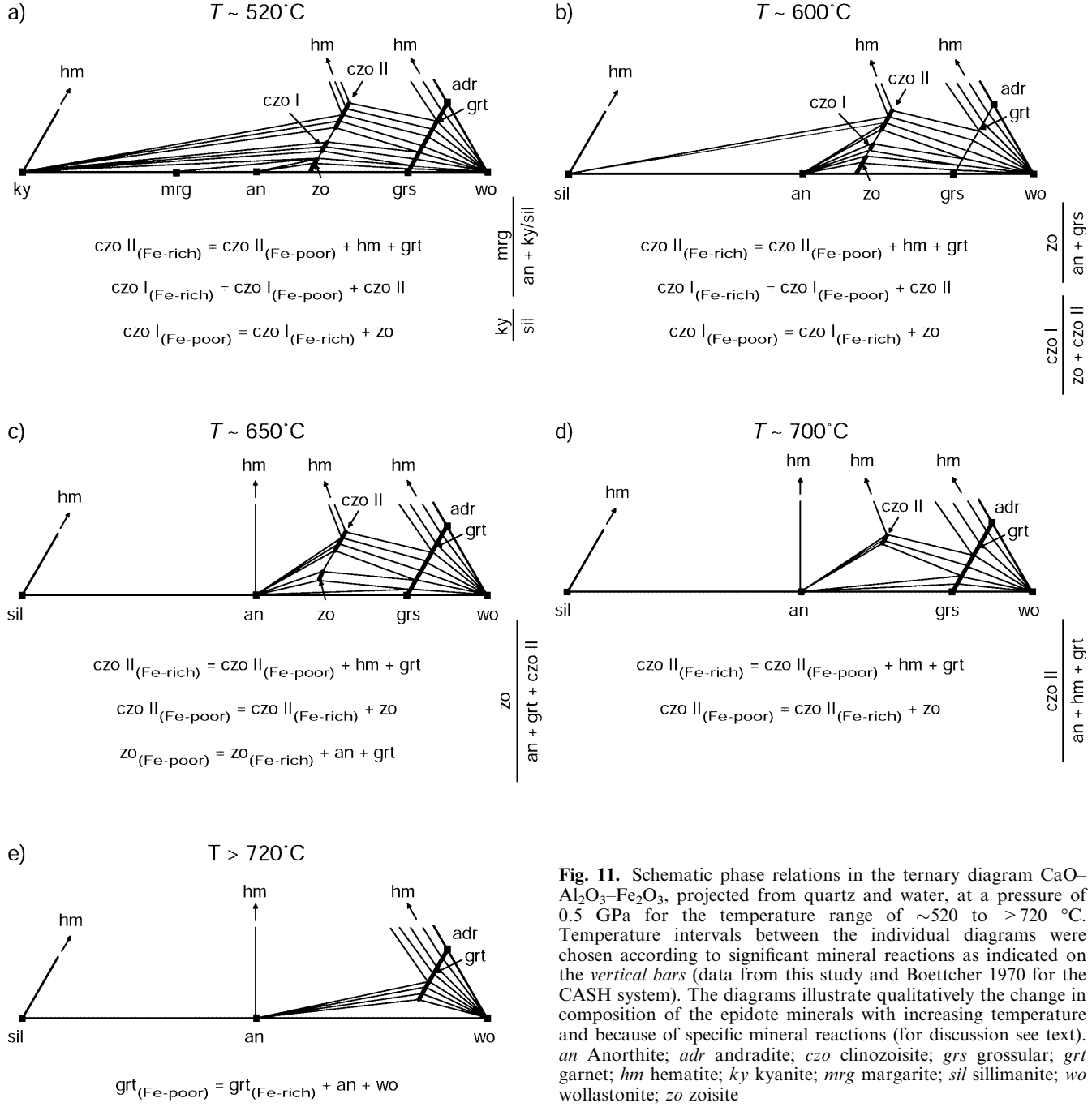

Fig. 11. Schematic phase relations in the ternary diagram CaO–Al_2O_3–Fe_2O_3, projected from quartz and water, at a pressure of 0.5 GPa for the temperature range of ~520 to >720 °C. Temperature intervals between the individual diagrams were chosen according to significant mineral reactions as indicated on the *vertical bars* (data from this study and Boettcher 1970 for the CASH system). The diagrams illustrate qualitatively the change in composition of the epidote minerals with increasing temperature and because of specific mineral reactions (for discussion see text). *an* Anorthite; *adr* andradite; *czo* clinozoisite; *grs* grossular; *grt* garnet; *hm* hematite; *ky* kyanite; *mrg* margarite; *sil* sillimanite; *wo* wollastonite; *zo* zoisite

czo II' two-phase field with a second miscibility gap, as found by Raith (1976) and Heuss-Aßbichler and Fehr (1997) between approximately $X_{ps} = 0.5$ and 0.7 to 0.8, might explain such a wide miscibility gap. According to our data (czo II overgrowths with $X_{ps}^{czoII} \sim 0.55$ and 0.6 at 0.5 GPa/500 °C), this intersection must occur at temperatures below 500 °C. Unfortunately, it seems unlikely that an experimental answer will be found to this problem because of the well-known sluggish reactions in the CFASH system, which make reliable results at temperatures below 500 °C unlikely. In accordance with our interpretation, Strens (1963) reports conditions of formation as low as 250 °C at 0.1 GPa.

Phase relations of the epidote minerals at 0.5 GPa

Experimental results of phase relations at 0.5 GPa are presented in a series of schematic $CaO–Al_2O_3–Fe_2O_3$ diagrams, projected from quartz and water (Fig. 11). The temperature intervals of Fig. 11 were chosen according to our data and those of Boettcher (1970) for the CASH system. At T ~520 °C (Fig. 11a), the three epidote minerals zoisite, clinozoisite I and clinozoisite II coexist with a grossular–andradite solid solution. Clinozoisite II with a near end member composition coexists with hematite and iron-rich garnet. In the aluminous portion of the system, margarite–anorthite–zoisite form a stable assemblage, but it is uncertain if margarite coexists with clinozoisite I or, as it is shown in Fig. 11a, kyanite with zoisite. At T ~600 °C (Fig. 11b), margarite has disappeared and yields anorthite and zoisite, which coexists with clinozoisite I. At T ~650 °C (Fig. 11c), clinozoisite I is the first of the three epidote minerals that disappears (see Fig. 3), and iron-rich zoisite coexists with clinozoisite II and anorthite or garnet. At this temperature, iron-free zoisite is already unstable. At T ~700 °C (Fig. 11d), zoisite has disappeared and clinozoisite II is the only epidote mineral, which finally becomes unstable, leaving anorthite–wollastonite–garnet and anorthite–hematite–garnet as the only assemblages (T > 720 °C, Fig. 11e).

It must clearly be stated that the application of these diagrams to natural assemblages must be made very carefully. Figure 11 is intended as a guide line for future studies, especially the investigation of natural assemblages to look for the respective composition of epidote minerals and garnet. Skarn assemblages should be very appropriate for such investigations for the high temperature region, whereas margarite–kyanite-bearing metasediments are promising for the low temperature region.

Acknowledgements The help of O. Appelt from GFZ-Potsdam with the EMP, and of H. Winkelmann from TU Berlin with the hydrothermal and piston cylinder laboratory, is gratefully acknowledged. This paper benefited from helpful discussions with M. Gottschalk, D. Lattard and S. Klemme and reviews by S. Poli and an anonymous reviewer. This work was funded by grant Fr 557/11-1,2 of the Deutsche Forschungs Gesellschaft (DFG) and is part of A.B.'s PhD thesis.

References

Berman RG (1988) Internally consistent thermodynamic data for minerals in the system $Na_2O–K_2O–CaO–MgO–FeO–Fe_2O_3–Al_2O_3–SiO_2–TiO_2–H_2O–CO_2$. J Petrol 29:445–522

Berman RG, Brown TH (1985) Heat capacity of minerals in the system $Na_2O–K_2O–CaO–MgO–FeO–Fe_2O_3–Al_2O_3–SiO_2–TiO_2–H_2O–CO_2$: representation, estimation, and high temperature extrapolation. Contrib Mineral Petrol 89:168–183

Bird DK, Cho M, Janik CJ, Liou JG, Caruso LJ (1988) Compositional, order/disorder, and stable isotope characteristics of Al–Fe epidote, State 2-14 Drill Hole, Salton Sea Geothermal System. J Geophys Res 93:13135–13144

Boettcher AL (1970) The system $CaO–Al_2O_3–SiO_2–H_2O$ at high pressures and temperatures. J Petrol 11:337–379

Brastad K (1985) Sr metasomatism and partition of Sr between the mineral phases of a meta-eclogite from Björkedalen, West Norway. Tschermaks Mineral Petrol Mitt 34:87–103

Brunsmann A (2000) Strukturelle, kristallchemische und phasenpetrologische Untersuchungen an synthetischen und natürlichen Zoisit- und Klinozoisit-Mischkristallen. PhD Thesis, Technical University of Berlin, Berlin http://edocs.tu-berlin.de/diss/2000/brunsmann_axel.pdf

Brunsmann A, Franz G, Erzinger J, Landwehr D (2000) Zoisite- and clinozoisite-segregations in metabasites (Tauern Window, Austria) as evidence for high-pressure fluid–rock interaction. J Metamorph Geol 18:1–21

Chatterjee ND, Johannes W, Leistner H (1984) The system $CaO–Al_2O_3–SiO_2–H_2O$: new phase equilibria data, some calculated phase relations, and their petrological applications. Contrib Mineral Petrol 88:1–13

Comodi P, Zanazzi PF (1997) The pressure behavior of clinozoisite and zoisite: an X-ray diffraction study. Am Mineral 82:61–68

Deer WA, Howie RA, Zussman J (1986) Epidote group. In: Deer WA, Howie RA, Zussman J (eds) Disilicates and ring silicates, 2nd edn. Longman Scientific and Technical, London, pp 2–179

Enami M, Banno S (1980) Zoisite–clinozoisite relations in low- to medium-grade high-pressure metamorphic rocks and their implications. Mineral Mag 43:1005–1013

Fehr KT, Heuss-Aßbichler S (1997) Intracrystalline equilibria and immiscibility along the join clinozoisite–epidote: an experimental and 57Fe Mössbauer study. N Jahrb Mineral Abh 172:43–67

Franz G, Selverstone J (1992) An empirical phase diagram for the clinozoisite-zoisite transformation in the system $Ca_2Al_3Si_3O_{12}(OH)–Ca_2Al_2Fe^{3+}Si_3O_{12}(OH)$. Am Mineral 77:631–642

Gottschalk M (1997) Internally consistent thermodynamic data for rock forming minerals. Eur J Mineral 9:175–223

Helgeson HC, Delany JM, Nesbitt HW, Bird DK (1978) Summary and critique of the thermodynamic properties of rock-forming minerals. Am J Sci 278A:1–229

Hemingway BS, Haas JL, Robinson GR (1982) Thermodynamical properties of selected minerals in the system $Al_2O_3–CaO–SiO_2–H_2O$ at 298.15 K and 1 bar (10^5 pascal) pressure and at higher temperatures. Geol Surv Bull 1544:1–70

Heuss-Aßbichler S, Fehr KT (1997) Intercrystalline exchange of Al and Fe^{3+} between grossular–andradite and clinozoisite–epidote solid solutions. N Jahrb Mineral Abh 172:69–100

Hietanen A (1974) Amphibole pairs, epidote minerals, chlorite, and plagioclase in metamorphic rocks, northern Sierra Nevada, California. Am Mineral 59:22–40

Holdaway MJ (1972) Thermal stability of Al -Fe epidote as a function of f_{O_2} and Fe content. Contrib Mineral Petrol 37:307–340

Holland TJB (1984) Stability relations of clino- and orthozoisite. In: Henderson CMB (ed) Progress in experimental petrology. The Natural Environment Research Council. Publication Series D no. 25, pp 185–186

Holland TJB, Powell R (1990) An enlarged and updated internally consistent thermodynamic dataset with uncertainties and correlations: the system $K_2O–Na_2O–CaO–MgO–MnO–FeO–$

Fe_2O_3–Al_2O_3–TiO_2–SiO_2–C–H–O_2. J Metamorph Geol 8:89–124

Jenkins DM, Newton RC, Goldsmith JR (1983) Fe-free clinozoisite stability relative to zoisite. Nature 304:622–623

Jenkins DM, Newton RC, Goldsmith JR (1985) Relative stability of Fe-free zoisite and clinozoisite. J Geol 93:663–672

Liou JG, Kim HS, Maruyama S (1983) Prehnite–epidote equilibria and their petrologic applications. J Petrol 24:321–342

Melzer S, Gottschalk M, Heinrich W (1998) Experimentally determined partitioning of Rb between richterites and aqueous (Na, K)-chloride solutions. Contrib Mineral Petrol 133:315–328

Nagasaki A, Enami M (1998) Sr-bearing zoisite and epidote in ultra-high pressure (UHP) metamorphic rocks from the Su-Lu province, eastern China: an important Sr reservoir under UHP conditions. Am Mineral 83:240–247

Newton RC (1965) The thermal stability of zoisite. J Geol 73:431–441

Newton RC (1966) Some calc–silicate equilibrium relations. Am J Sci 264:204–222

Pawley AR, Redfern SAT, Holland TJB (1996) Volume behavior of hydrous minerals at high pressure and temperature: I. thermal expansion of lawsonite, zoisite, clinozoisite, and diaspore. Am Mineral 81:335–340

Poli S, Schmidt MW (1998) The high pressure stability of zoisite and phase relationships of zoisite-bearing assemblages. Contrib Mineral Petrol 130:162–175

Prunier AR Jr, Hewitt DA (1985) Experimental observations on coexisting clinozoisite and zoisite. Am Mineral 70:375–378

Raith M (1976) The Al–Fe(III) epidote miscibility gap in a metamorphic profile through the Penninic series of the Tauern Window. Contrib Mineral Petrol 57:99–117

Schmidt MW, Poli S (1994) The stability of lawsonite and zoisite at high pressures: experiments in CASH to 92 kbar and implications for the presence of hydrous phases in subducted lithosphere. Earth Planet Sci Lett 124:105–118

Selverstone J, Spear FS (1985) Metamorphic P–T paths from pelitic schists and greenstones from the south-west Tauern Window, Eastern Alps. J Metamorph Geol 3:439–465

Strens RGJ (1963) Some relationships between members of the epidote group. Nature 198:80–81

Strens RGJ (1964) Epidotes of the Borrowdale Volcanic rocks of central Borrowdale. Mineral Mag 33:868–886

Winkler HGF, Nitsch KH (1962) Zoisitbildung bei der experimentellen Metamorphose. Naturwissenschaften 49:605

Zimmermann R, Heinrich W, Franz G (1996) Tremolite synthesis from $CaCl_2$-bearing aqueous solutions. Eur J Mineral 8:767–776